ARTICLE

# New Insights into Proton Surface Mobility Processes in PEMFC Catalysts Using Isotopic Exchange Methods

**Paloma Ferreira-Aparicio***

Centro de Investigaciones Energéticas, Medioambientales y Tecnológicas (CIEMAT), Avenida Complutense 22, 28040 Madrid, Spain

**ABSTRACT** The surface chemistry and the adsorption/desorption/exchange behavior of a proton-exchange membrane fuel cell catalyst are analyzed as a case study for the development of tailor-made support materials of enhanced performance and stability. By using $H_2$, $D_2$, and CO as probe molecules, the relevance of some surface functional groups of the catalyst support on several diffusion processes taking place during the adsorption is shown. Sulfonic groups associated with the vulcanized carbon black surface have been detected by means of spectroscopic techniques (X-ray photoelectron spectroscopy and Fourier transform infrared spectroscopy) and by analysis of the desorbed products during temperature-programmed desorption tests by mass spectrometry. Such hydrophilic species have been observed to favor proton surface mobility and exchange with Pt-adsorbed deuterium even in the presence of adsorbed CO. This behavior is relevant both for the proper characterization of these kinds of catalysts using adsorption probes and for the design of new surface-modified carbon supports, enabling alternative proton-transfer pathways throughout the catalytic layers toward the membrane.

**KEYWORDS:** Pt/Vulcan XC72 • chemisorption • $D_2$ isotopic exchange • $D_2$—CO coadsorption • PEMFC catalyst

## INTRODUCTION

The state-of-the-art proton-exchange membrane fuel cell (PEMFC) catalysts typically consist of Pt nanoparticles (2—8 nm) dispersed on a high-surface-support material that provides a good combination of electron conductivity, corrosion resistance, surface properties, and low cost (1, 2). Pt loadings in these catalysts are usually in the range between 20 and 60 wt %. Numerous carbon materials including carbon aerogels (3), cryogels (4), a large variety of carbon blacks (CBs) (5), high-surface-area graphites (6), single-wall and multiwall carbon nanotubes (7, 8), graphitic carbon nanofibers (8, 9), carbon nanohorns (7, 10), carbon nanocoils (11), and ordered uniform porous carbon networks (12) have been used as supports to synthesize them. Despite the numerous attempts at looking for materials providing high-performance catalysts with low corrosion rates, the traditionally used Vulcan XC72 CB remains as the most popular and extensively used material because of its superior behavior in catalysts for PEMFCs (9—17).

The Vulcan XC72 CB and PEMFC catalysts prepared on it have been extensively studied in electrochemical devices (18—32) but there is scarce information about their surface properties (33, 34). Just a few papers can be found regarding the particularities of the surface chemistry of this CB or its composites (35—38), dealing with the effects that the surface functional groups confer to the Pt nanoparticles in the surroundings, or analyzing the Pt-support synergy, especially in catalysts with high metal loadings (39—45). Most of these studies are mainly focused in O-containing groups (39, 45, 46), and little attention is paid to surface species containing other heteroatoms (34, 47), which are relevant for some catalyst properties, such as their activity and durability.

A number of reviews related to the degradation mechanisms affecting the activity and durability of C-supported Pt catalysts in PEMFC electrodes have been recently published (41, 42, 45, 48—52). In general, the strategies proposed for improving the catalyst durability involve increasing the graphitization degree of the supports, modifying their surface chemistry by building proper surface functional groups, increasing the density of the basic sites on carbon supports to enhance the Pt—C interaction, increasing the surface stability of the C support, improving the hydrophobicity of the C support through proper surface treatment, and preparing catalysts with high Pt uniformity and low Pt load. As a matter of fact, some new trends in PEMFC catalyst research follow these strategies by applying sulfonation treatments (53—56) or modifying the C surface with sulfonated polymers (44, 57, 47). The introduction of surface functional groups on the C surface induces properties and characteristics in the supports and catalysts that must be carefully analyzed, especially regarding their thermal stability (33, 45) and their behavior under different atmospheres (46, 58, 59). C functional groups like carboxyls, lactones, anhydrides, carbonyls, phenols, quinones, or lactones do not exert, in general, a beneficial effect on PEMFC catalysts (45, 60). Anchoring of the metal precursor is improved in the presence of O-containing groups during the catalyst synthesis process, but some drawbacks must be considered. They can both decrease the conductivity of catalysts and weaken the

* E-mail: paloma.ferreira@ciemat.es.
Received for review May 20, 2009 and accepted July 30, 2009
DOI: 10.1021/am9003446



Published on Web 08/26/2009

interaction between the support and the catalytic metal nanoparticles, resulting in an accelerated metal sintering. Furthermore, they contribute to increased hydrophilicity in the electrodes with subsequent repercussion on the water and gas-transport mechanisms.

This work analyzes in detail the surface chemistry of the most widely used CB for PEMFC catalysts. Particular attention is paid to some scarcely explored issues on these types of catalysts: the interaction of probes with surface groups and the thermal stability of surface species. The modification of the thermal stability of species associated with the Vulcan XC72 surface as a result of the presence of Pt nanoparticles, and under atmospheres containing $H_2$ or $H_2$ and CO, is discussed in light of the presented results. These results are presented as a case study for developing tailor-made surface-modified supports for PEMFC catalysts of improved performance. The adsorption and exchange behavior of these kinds of catalysts in gas diffusion electrodes (GDEs) is also analyzed to evaluate the participation of those groups in the proton surface mobility within the catalytic layer.

## EXPERIMENTAL SECTION

A standard Pt (20 wt %) supported on a Vulcan XC72 catalyst from E-TEK has been used for characterization of its surface chemistry and adsorption properties. Some additional experiments have been carried out on Vulcan XC72 CB (Cabot Corp.) as a reference for the bare support. The adsorption/desorption and exchange experiments have been performed in a calibrated glass volumetric system equipped with a turbomolecular pump, a Pirani vacuum sensor, and a Baratron capacitance manometer. A quadrupole mass spectrometer (Quadstar QMS 200 M2) with channeltron and faraday detectors was coupled to the system for analysis of its gaseous atmosphere.

Surface functional groups on the catalyst and the pristine support have been studied by mass spectrometric analysis of the gas phase during temperature-programmed desorption (TPD) tests and by Fourier transform infrared (FTIR) spectroscopic analysis in the transmission mode. For TPD experiments, aliquots of 25−50 mg of sample were placed in a glass bulb and treated under vacuum at 298 K for 15 min. Then, they were heated under a dynamic vacuum with a linear temperature ramp of $10\ K \cdot min^{-1}$, and the desorbed species were analyzed. Ion currents for a number of mass-to-charge ratios between 2 and 100 were collected on an interfaced computer. The global pressure in the chamber was registered by a pressure transducer connected to the mass spectrometer inlet. FTIR spectroscopic analysis was performed on wafers prepared by mixing of the catalyst or the CB support with 95 wt % of dehydrated KBr. The thermal stability of the functional groups in the samples was analyzed by applying a thermal treatment to the wafers.

Additional X-ray photoelectron spectroscopy (XPS) analysis of the Vulcan XC72 CB was performed in a Perkin-Elmer PHI 5400 spectrometer. The excitation source was the Mg Kα line ($h\nu = 1253.6$ eV) with a spot size of 1 $mm^2$. The pressure in the analysis chamber was kept below $10^{-9}$ Torr during acquisition.

Isotopic exchange tests have been carried out on fresh catalyst samples at 298 K under a controlled atmosphere using $D_2$ as the probe molecule. $D_2$ (isotopic purity ≥99.8%) was purchased from Cambridge Isotope Laboratories, Inc. By means of the exchange process, the participation of the surface functional groups with exchangeable $H_2$ has been analyzed. For the experiment, a pressure of 21 mbar was admitted in the vacuum chamber and contacted with the sample while analyzing the changes in the gas-phase composition with time. A leak valve in the quadrupole mass spectrometer inlet kept the reduction of the amount of gas admitted for the analysis to a minimum and maintenance of the pressure in the sample chamber to remain practically unchanged. The exchange capacity of the catalyst and the rate of the process have been determined from a decrease of the ion current for the mass 4 ($D_2$) and an increase of the ion current for masses 3 (HD) and 2 ($H_2$) in the mass spectrometer.

Adsorption properties were evaluated by the chemisorption of $H_2$, $D_2$, and/or CO as probe molecules. Different pretreatment temperatures have been applied to explore the impact of the remaining surface groups in the adsorption behavior. For adsorption measurements, samples of 30 mg were charged in a glass bulb connected to the volumetric adsorption system. After evacuation of the air in the bulb, the sample was heated at a given temperature under a dynamic vacuum and maintained for 2 h under those conditions. Then, it was cooled at 298 K and the adsorption isotherm was measured with $H_2$ or CO. The chemisorbed amount was calculated by extrapolation of the linear part of the isotherm curve to zero equilibrium pressure.

In some cases, after measurement of the $H_2$ adsorption isotherm, the sample was contacted with air to oxidize Pt-chemisorbed $H_2$ and a new adsorption cycle was performed, treating the sample again under a dynamic vacuum for 2 h at the same temperature as before. Then, a new $H_2$ adsorption isotherm was measured at 298 K. These cycles were repeated until a constant $H_2$ uptake was obtained. A fresh sample of the catalyst was used for each adsorption test using a given pretreatment temperature.

In order to explore the $D_2$ exchange ability of the sample when surface Pt is blocked with a monolayer of CO, a coadsorption experiment was performed. $D_2$ was admitted into the bulb under vacuum over a CO-equilibrated sample of the catalyst. After an equilibration period of 10 min, the residual gas in the chamber was removed and the sample maintained under a dynamic vacuum for 15 min. Then, the species that evolved during the TPD were analyzed.

Additional characterization of the catalyst has been performed by X-ray diffraction (XRD) and transmission electron microscopy (TEM) in order to compare the surface metal areas obtained by different techniques. XRD analysis was carried out on the fresh catalyst to evaluate the average Pt particle size. A volume average diameter was estimated from the broadening of the Pt XRD line corresponding to the (220) plane ($2\theta = 65.7°$). Diffractograms were recorded in a Seifert XRD 3000P instrument in the 4−90° $2\theta$ range in a continuous scan mode with Cu Kα radiation ($\lambda = 1.540\ 598$ Å). TEM was also carried out in the catalyst to obtain direct images of individual Pt particles representative of the sample structure. A 200 kV Jeol JEM-2100F microscope with a probe size under 0.5 nm has been used for the analysis. A sample of the catalyst was ultrasonically dispersed in acetone and spread over perforated Cu microgrids. Numerous micrographs of different portions of the sample were obtained for the statistical determination of the mean Pt particle size.

$H_2$ adsorption and $D_2$ exchange rate measurements have also been carried out in GDEs containing Pt/Vulcan XC72 as references for a comparison with the results obtained with the catalyst. Two GDEs have been prepared with the standard Pt (20 wt %)/Vulcan XC72 catalyst from E-TEK. Two different inks containing a Nafion perfluorinated ion-exchange resin (Aldrich, 5 wt % solution) were prepared with distinct solvents for deposition of the catalytic layers. One of them was dissolved in isopropyl alcohol and the other in a mixture of butyl acetate, ethanol, and glycerol in a proportion of 45:50:5. The percentage of resin in the catalytic layer was 30%. The third electrode was a commercial GDE from E-TEK (LT-140E-W ELAT). All of the GDEs had a catalyst loading of 0.5 $mg_{Pt} \cdot cm^{-2}$.

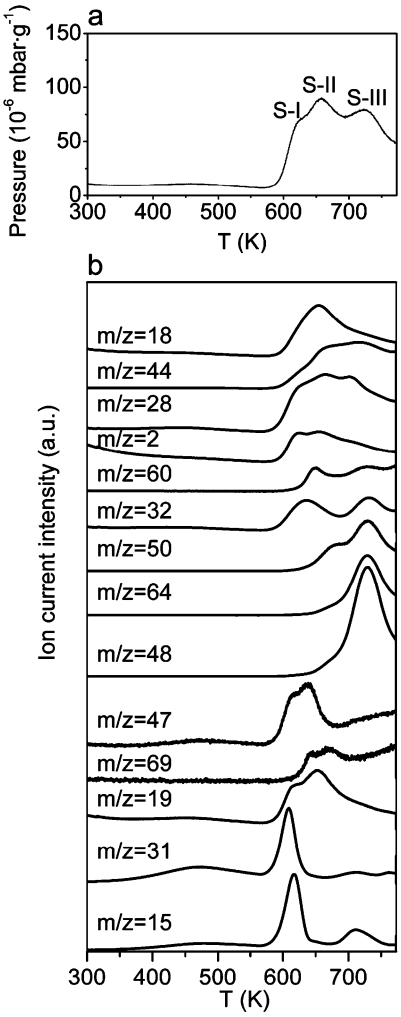


**FIGURE 1. TPD profiles for the pristine Vulcan XC72 CB under a dynamic vacuum: (a) pressure increase in the analysis chamber; (b) ion current profiles corresponding to the mass spectrometric analysis of desorbed species.**

## RESULTS AND DISCUSSION

**Surface Chemistry of the Support.** By analysis of the thermal desorption profiles of a pristine sample of Vulcan XC72 under vacuum, some particular characteristics can be found in this CB concerning its support surface groups. Figure 1a shows the TPD curve obtained from the pressure increase in the vacuum chamber resulting from decomposition of the surface species when the sample was heated up to 773 K. Three main desorption processes can be distinguished between 600 and 753 K. The ion current profiles registered in the mass spectrometer for the most significative *m*/*z* ratios contributing to the global pressure increase are presented in Figure 1b. At the lowest temperature, ion currents corresponding to species like $CF_x^+$ (*m*/*z* 19, 31, 50, and 69), $CH_y^+$ (*m*/*z* 15), $H_2^+$ (*m*/*z* 2), $CO^+$ (*m*/*z* 28), and $COF^+$ (*m*/*z* 47) increase. The ion current intensity for *m*/*z* 19, which can be assignable to $F^+$ ions, contains an important contribution from $H_2O$ (*m*/*z* 18) as the secondary mass. The differences existing between the profiles for masses 18 ($H_2O^+$) and 19 (naturally occurring isotopes of $H_2O^+$, $H_3O^+$, and $F^+$), which concur with the increase of the ion current intensity for the mass *m*/*z* 31, confirm the presence of $F^+$ species. The formation of a more intense peak at ca. 660 K (S-II in Figure 1a) corresponds mainly to $H_2O$ release (*m*/*z* 18), although there is also a contribution of CO (*m*/*z* 28) and some S-containing compounds, such as COS (*m*/*z* 60). The third peak (S-III in Figure 1a) is mainly due to $CO_2$ and $SO_2$ with contributions of several ion currents (*m*/*z* 64, 48, 50, and 32).

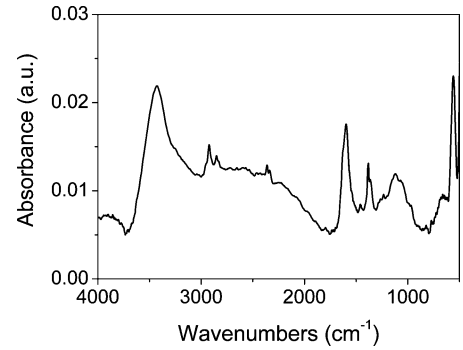


**FIGURE 2. FTIR spectra obtained for the pristine Vulcan XC72 CB.**

F- and S-containing species have been detected on the CB support by FTIR (Figure 2). The spectral IR features obtained for the CB in the range between 2000 and 500 $cm^{-1}$ confirm their presence. The assignment of IR bands corresponding to $CF_x$ species and sulfonic groups has been made by a comparison with those reported in the literature for fluorided C materials (75, 62) and fluoropolymers (63−71). Two main regions with bands between 750 and 500 $cm^{-1}$ and between 1300 and 900 $cm^{-1}$ can be attributed to characteristic IR absorption modes for $CF_x$ species and sulfonic groups. Symmetric and asymmetric stretching bands of C−F bonds appear at ca. 1154 and 1230 $cm^{-1}$, respectively. Several vibration frequencies of O-containing groups probably present on the CB surface also lie in this region. These species are probably contributing to poorly defined peaks in overlapped bands. The absorption peaks lying in this frequency range can be ascribed to $-SO_2OH$ groups with characteristic vibration modes at 970, 1150, 1230, and 1425 $cm^{-1}$ (71). No clear bands can be assigned to the asymmetric stretching of $-SO_3^-$ in the 1300−1320 $cm^{-1}$ region (72, 73). However, their presence cannot be completely ruled out because of the numerous low-intensity absorption bands in the spectrum. According to the literature, when a substituent, C═O, is directly conjugated to aromatic rings, a doublet is observed at 1625−1575 $cm^{-1}$ (74). On the basis of this consideration, the strong band centered at ca. 1590 $cm^{-1}$ in Figure 2 can be assigned to quinone groups in Vulcan XC72 (75, 76). Aromatic C═C stretching vibrations such as naphthalene- or anthracene-like structures also lie in the same region, resulting in bands within 1620−1580 and 1550−1505 $cm^{-1}$. Bands corresponding to the different $CH_x$ absorption modes can be also identified at 1465, 1380, and 720 $cm^{-1}$ together with the C−H stretching vibrations in the low-frequency region between 2950 and 2850 $cm^{-1}$. The bands at 2926 and 2952 $cm^{-1}$ correspond to the asymmetrical C−H stretching modes of $-CH_2$ and $-CH_3$ groups, respectively, and that centered at 2856 $cm^{-1}$ corresponds to their symmetrical C−H stretching modes. The strong and

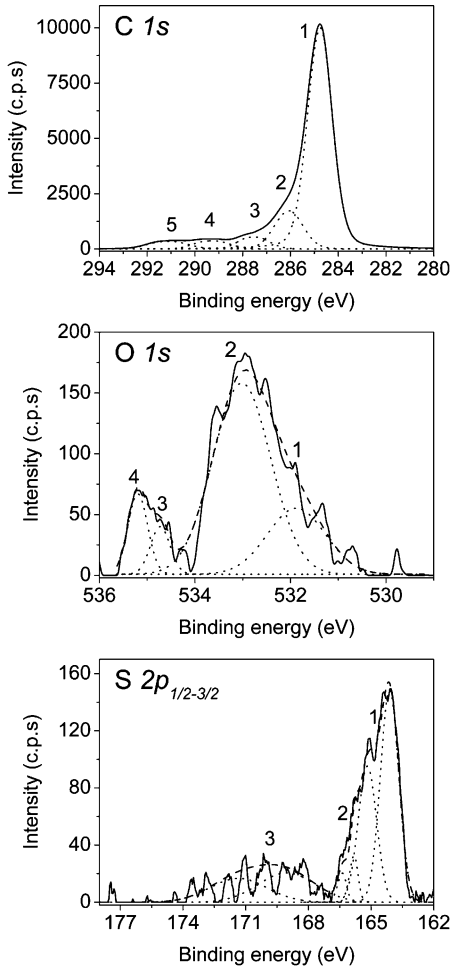


**FIGURE 3. XPS spectra of the Vulcan XC72 CB in the C 1s, O 1s, and S 2p regions.**

broad band at ca. 3428 $cm^{-1}$ in Figure 2b reveals the presence of adsorbed $H_2O$. In addition to the $H_2O$ stretching vibration, the contribution due to its bending mode is probably superposed to the bands previously assigned to quinone groups in the region of ca. 1590 $cm^{-1}$.

XPS analysis of the CB indicates a surface composition corresponding to C, O, and S in atomic proportions of 99.3, 0.5, and 0.2%. F has not been evaluated because of a very weak signal partially masked by the noise. Its low concentration in combination with a defluorination process induced by the X-ray radiation is one of the problems making its detection difficult. Halogen-containing compounds have been found to be especially sensitive to X-ray exposure, resulting in a decrease in the halogen peak intensity and an increase in the C 1s signal (77−80). Figure 3 shows the signals in the binding-energy regions corresponding to C 1s, O 1s, and S 2p.

The main C 1s signal from Vulcan XC72 is observed at an energy of 287.4 eV (74.1%) probably due to C−C/C−H bonds. A broad contribution at higher binding energy was deconvoluted into four contributions at 286.1 and (13.9%), 287.4 (4.6%), 289.2 (3.6%), 291.0 (3.8%) eV, which can be assigned to −COH, −C═O, −COOH or −CF, and $CF_2$ groups, respectively (78−80). The O 1s signal could be fitted into four components located at approximately 532, 533, 534.5,

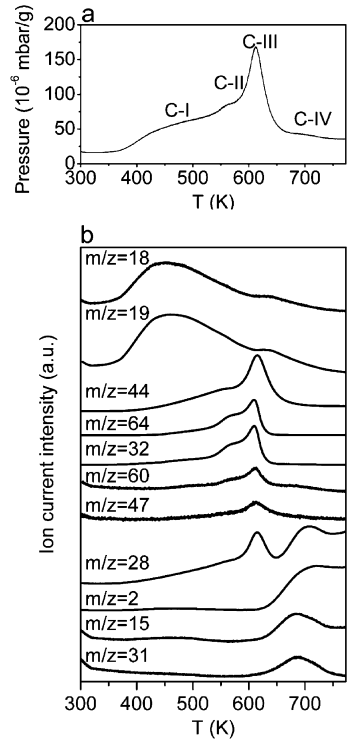


**FIGURE 4. TPD profile for the Pt/Vulcan XC72 catalyst under a dynamic vacuum: (a) pressure increase in the analysis chamber; (b) ion current profiles corresponding to the mass spectrometric analysis of desorbed species.**

and 535.2 eV, which could be attributed to −C═*O*, −C−*O*−, −*O*−C═O, and $-SO_3^-$ type groups, respectively (80). Although the signal-to-noise ratio was low at the S 2p region, at least two main contributions were identified: the main one at 164.7 eV and the other at 170.4 eV. The signal has been fitted to Gaussian line shapes. For resolution of each S $2p_{1/2-3/2}$ doublet, the intensity ratio of the two components was required to be 1:2 and their widths to be the same. Poleunis et al. have attributed the most intense S 2p signal at 164.7 eV to thiolate groups (−SH) (34) on Vulcan XC72. The contribution of S atoms with double bonds to C atoms (S═C═S) with typical binding energies at 164 eV cannot be excluded (81). It is well-known that vulcanization processes in CBs involve reactions with S, leading to the formation of S═C═S species.

The signal at 170.4 eV can be assigned to sulfonic groups ($-SO_2OH$) (56, 82, 83). For the best fit of the S $2p_{1/2-3/2}$ doublets, a third contribution was found at a binding energy of 166.2 eV, which could be associated with the sulfite state. It has been reported that sulfur mutates from the sulfonic acid group configuration to a sulfite state induced by irradiation by X-ray or ions (82).

**Surface Chemistry of the Catalyst.** The species resulting from decomposition of the surface groups in the catalyst have been analyzed by mass spectrometry in an analogous way. The desorption takes place in at least four well-defined processes (peaks C-I−C-IV) between 370 and 740 K, as revealed by the pressure variation profile in Figure 4a. The most defined and intense peak is the third one (C-III) centered at ca. 610 K. The most significant contributions

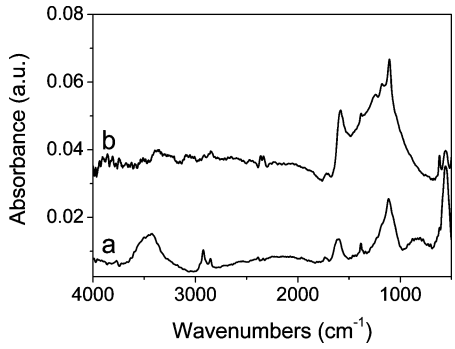


**FIGURE 5. FTIR spectra obtained for the pristine Pt/Vulcan XC72 catalyst as received (a) and after its treatment under vacuum at 448 K (b).**

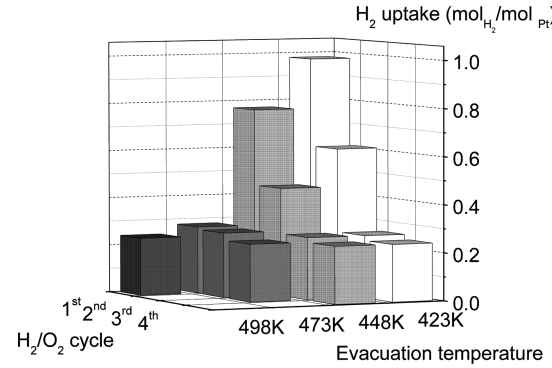


**FIGURE 6. $H_2$ uptake per 1 mol of Pt for the Pt/Vulcan XC72 catalyst as a function of the number of cycles of $H_2$ adsorption/$O_2$ adsorption and the temperature of treatment under vacuum before $H_2$ adsorption.**

to the TPD curve resulting from the catalyst, as revealed by mass spectrometry, are presented in Figure 4b.

A detailed analysis of a number of *m*/*z* ratios and their profiles allows the determination of the nature of the main chemical species released at each temperature: the C-I peak (Figure 4b) is mainly due to the release of $H_2O$ (*m*/*z* 18); peaks C-II and C-III can be assigned to the simultaneous evolution of $CO_2$ (*m*/*z* 44 and 28), $SO_2$ (*m*/*z* 64 and 32), and COS (*m*/*z* 60 and 28), and finally the broad C-IV peak corresponds to the formation of $CF_x$ (*m*/*z* 31) and $CH_y$ (*m*/*z* 15) species, $H_2$ (*m*/*z* 2), and CO (*m*/*z* 28). All of these species have been previously detected during the TPD of the support (Figure 1b), but their decomposition profiles differ substantially in the presence of Pt nanoparticles.

The IR features of the catalyst in its pristine form and after treatment in a vacuum at 448 K are presented in Figure 5. The main IR absorption bands present in the support are also found in the IR spectrum of the catalyst. However, there is a general change in its profile, which is probably the result of the change in the proportion of S- and F-containing groups after Pt incorporation. This change is even more evident when the catalyst is treated under vacuum at 448 K. According to the thermal desorption curve in Figure 4, the treatment of the catalyst at that temperature just leads to the release of most of the adsorbed $H_2O$ without influencing the decomposition of other surface species. As a matter of fact, the broad absorption band in the region ca. 3400 $cm^{-1}$ due to the fundamental stretching vibration of $H_2O$ becomes dramatically reduced after heating of the catalyst at 448 K (Figure 5b). In the region 500−1650 $cm^{-1}$, numerous absorption bands attributable to the vibration frequencies of fluorocarbon species and sulfonic and carbonyl groups can be observed. Absorption modes attributable to $-SO_2OH$ groups with characteristic vibrations at ca. 970, 1150, 1230, and 1425 $cm^{-1}$ are probably overlapped with other IR vibrations corresponding to C−F and C−O−C bonds lying in the same range and leading to a broad absorption band in that region (71−73).

**Adsorption-Exchange Properties of the Catalyst.** The adsorption properties of the Pt/Vulcan XC72 catalyst have been evaluated by means of different procedures using $H_2$ and CO as probe molecules. The influence of the support surface groups on the adsorption processes has been analyzed on catalyst samples subjected to different thermal treatments. To enlighten the participation of the surface groups of the support in the adsorptive properties of the catalyst, exchange experiments with isotopically labeled molecules have been performed.

**a. $H_2$ Chemisorption on Pt/Vulcan XC72.** The static volumetric method of adsorption in the Pt/Vulcan XC72 catalyst leads to variable $H_2$ uptakes at 298 K depending on the thermal treatment of the sample. $H_2$ uptakes obtained on the pristine catalyst after being treated under vacuum at temperatures as low as 423 K correspond to atomic ratios of H/Pt close to 2.0, where Pt is refers to the total amount of Pt in the catalyst. This large ratio reveals that adsorption phenomena induced by groups on the support surface are taking place simultaneously with the $H_2$ chemisorption on the metal surface. Those processes interfere with $H_2$ chemisorption measurements and make determination of the surface Pt difficult. The contribution of parallel adsorption phenomena masking the authentic $H_2$ chemisorption on the surface Pt has been minimized by applying increasing pretreatment temperatures in pristine samples and/or successive $H_2/O_2$ titration cycles to oxidize only Pt-chemisorbed $H_2$. As shown in Figure 6, both procedures are effective in reducing $H_2$ uptakes to a constant value of 0.24 mol of $H_2$ per 1 mol of Pt in the catalyst. The Pt dispersion, defined as the percentage of surface Pt related to the total Pt in the catalyst, is 48%. Assuming that the Pt particles have a spherical geometry and that their surface is formed by equal proportions of the main low-index planes (84), an average Pt particle size of 2.4 ± 0.2 nm has been estimated.

In order to verify the validity of that measurement as the actual $H_2$ chemisorption on Pt, the average Pt particle size estimated from the $H_2$ uptake has been compared with those obtained from the pristine catalyst using XRD and TEM techniques. Both the analysis of the broadening of the XRD line corresponding to the Pt(220) plane ($2\theta = 65.7°$) and the analysis of the particle size distribution from TEM micrographs yield mean crystallite sizes slightly above that estimated from the $H_2$ chemisorbed amount. For the statistical determination of the mean Pt particle size from TEM micrographs, numerous samples representative of the catalyst, accounting for several hundreds of particles, have been

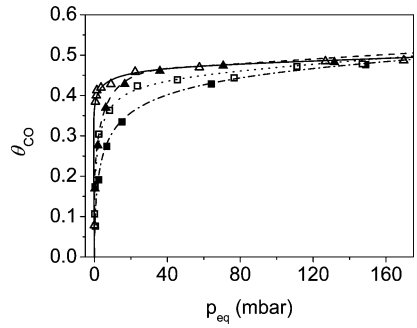


**FIGURE 7. CO adsorption isotherms on the Pt/Vulcan XC72 catalyst after its evacuation at (■) 423 K, (□) 448 K, (▲) 473 K, and (△) 648 K.**

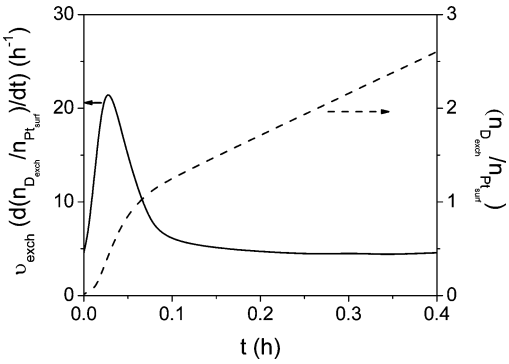


**FIGURE 8. $D_2/H_2$ exchange frequency ($\nu_{exch}$) (solid line) and amount of moles of D atoms exchanged per 1 mol of surface Pt (dashed line) in the Pt/CB catalyst as a function of the contact time between the gas and the sample at 298 K. The catalyst has been previously treated under a dynamic vacuum at 448 K for 1 h.**

examined. More than 50% of the measured particles have mean diameters in the range between 2.4 and 3.9 nm, resulting in somewhat larger particles than when measured by means of XRD. By analysis of the broadening of the Pt XRD lines, the estimated volume average diameter is found to be 2.7 ± 0.3 nm. The somewhat larger size obtained by TEM is probably a consequence of the poorer representation of the smallest particles in the micrographs, which usually leads to an overestimation of the average diameter. By using the XRD technique, the estimated values can be affected by a significant error in the catalysts with large proportions of very small Pt particles or inhomogeneous particle size distributions. However, in this case, there is very good agreement among the three applied techniques for the Pt mean diameter estimations.

**b. CO Chemisorption on Pt/Vulcan XC72.** CO uptakes have also been determined on fresh catalyst samples after thermal treatment under vacuum. Using different evacuation temperatures, a constant value of 0.22 mol of CO per 1 mol of Pt is obtained independently of the applied pretreatment. According to the obtained values for the monolayer coverage using $H_2$ and CO as chemisorption probes, the resulting CO/H stoichiometry is close to 0.5. This ratio is lower than the typical 0.7 saturation limit usually found in the literature for supported Pt particles, with low or no interaction with the supports showing adsorption surface properties of Pt(111) (85).

Although the CO uptakes seem to be unaffected by the presence of the support surface groups, the CO adsorption isotherms reveal the influence of the support surface chemistry on the adsorption of CO on the Pt crystallites dispersed on it. A detailed analysis of the CO adsorption isotherms on catalyst samples evacuated at different temperatures indicates that, as long as the support surface is progressively modified at increasing pretreatment temperature (mainly by dehydration), the CO isotherm profile changes (Figure 7). Although CO adsorption on Pt does not meet the premises of Langmuir's adsorption model (i.e., monolayer coverage, adsorption site equivalence, and no interaction among adsorbate molecules), its simplicity and strong theoretical reasoning makes it a good approach to describing the obtained isotherms. Considering that the curves approach the ideal model of a type I Langmuir isotherm at low equilibrium pressures, the CO adsorption strength related to the α adsorption constant in the Langmuir equation [$\theta_{CO} = \alpha p_{eq}/(1 + \alpha p_{eq})$] increases as long as the support surface groups are dehydrated at increasing pretreatment temperatures.

**c. Role of Surface Groups in Adsorption on Pt/Vulcan XC72.** Adsorption results shown in Figure 6 indicate that a parallel $H_2$ adsorption process takes place simultaneously with $H_2$ chemisorption on Pt when the catalyst has been evacuated at temperatures as low as 423 K. The mechanism of this phenomenon still remains an open question. To enlighten the nature of this process and the species involved in it, two types of experiments have been carried out: isotopic exchange under steady-state conditions and TPD tests after $D_2$ adsorption, CO adsorption, and CO−$D_2$ coadsorption.

The ability of the catalyst thermally treated at 448 K under vacuum to exchange $H_2$ species from its surface with molecular $H_2$ gas has been studied by mass spectrometry using $D_2$ as the probe molecule for adsorption. The extent of the surface $H_2$ mobility process has been evaluated by analysis of the composition of the gas phase during the contact time between pure $D_2$ gas and the Pt/Vulcan XC72 catalyst previously treated under a high vacuum at 448 K. The analysis of the gas-phase composition reveals how the ion current for $D_2$ (*m*/*z* 4) decreases whereas those for HD (*m*/*z* 3) and $H_2$ (*m*/*z* 2) ratios increase progressively when $D_2$ is circulated over the catalyst at 298 K. The observed $H_2$ exchange rate is presented in Figure 8 together with the ratio of exchanged atoms per surface Pt center. The exchange rate has been expressed as a turnover number by referring to the amount of D atoms exchanged to the Pt surface centers in the catalyst. Pt surface centers have been estimated from the $H_2$ chemisorption measurements performed on the catalyst. As shown in Figure 8, two processes taking place at different rates can be distinguished during the exchange test. The exchange turnover frequency is very fast during the initial period of contact (about 5 min), and then it reaches a steady state with a constant value of 4.9 $h^{-1}$. By analysis of the molar ratio of exchanged D per surface Pt, it can be observed that this ratio approaches unity during the first step. This indicates that the catalyst exchanges practically the whole monolayer of initially Pt-chemisorbed $D_2$, with the closest surface groups able to exchange $H_2$ species. There-

fore, the first process after contacting the catalyst with $D_2$ gas can be attributed to a relatively fast exchange between the first chemisorbed $D_2$ monolayer on nanometric Pt particles and the proton acceptor species on the support located close to their periphery. After that first step, the exchange rate is observed to decrease to a value that probably corresponds to the proton diffusion rate on the CB surface at 298 K.

This $D_2/H_2$ exchange process is often observed on catalysts with proton acceptor groups on the support surface. It has been previously shown that $H_2$ uptakes measured on this catalyst after vacuum treatment at soft temperatures largely surpass the Pt monolayer coverage. This enhanced $H_2$ adsorption, which is usually known as spillover, is usually ascribed to surface diffusion phenomena of $H_2$ species toward the support (39). This effect has already been reported for fuel cell catalysts (39, 87). Ramirez-Cuesta et al. have provided evidence of this phenomenon by means of inelastic neutron scattering spectroscopy on Pt/C, Ru/C, and PtRu/C (87, 88). The contribution of spilled-over $H_2$ to adsorption measurements can be eliminated by applying successive adsorption cycles of $H_2$ and $O_2$ until reaching a steady-state $H_2$ coverage. This procedure allows saturation of surface sites promoting spillover and just evaluation of surface Pt centers. The particular adsorption properties of Pt/Vulcan XC72 are induced by surface functional groups in the CB promoting hydrophilic and hydrophobic characteristics on its surface (39, 89, 90).

The adsorption of $D_2$ and CO as probe molecules has been carried out on catalyst aliquots previously evacuated at 448 K in order to analyze their desorption profiles. After treatment in a vacuum at that temperature, $D_2$ adsorption at 298 K includes a large contribution of spilled-over species. $D_2$ uptake increases from 1.24 $mmol \cdot g_{Pt}^{-1}$ (when no surface diffusion phenomena are involved in the measurement) to 3.95 $mmol \cdot g_{Pt}^{-1}$ for a pristine sample treated under a dynamic vacuum at 448 K for 1 h. On the other hand, the CO uptake for identical conditions is 1.08 $mmol \cdot g_{Pt}^{-1}$, which corresponds to a coverage close to 50% of the monolayer. An additional adsorption test was carried out on a CO-equilibrated sample. After saturation of its surface with CO at 298 K, the gas phase was removed and then $D_2$ was dosed. Under these conditions, the measured $D_2$ uptake corresponded to 2.05 $mmol \cdot g_{Pt}^{-1}$, indicating that the presence of CO does not block the $H_2$ diffusion pathways between the metal and the support surface groups.

Following each adsorption test, a TPD experiment was performed at 10 $K \cdot min^{-1}$ during analysis of the desorbed species. The pressure in the system was registered during the experiments. Figure 9 presents the global desorption profiles obtained from the catalyst after $D_2$ adsorption, after CO adsorption, and after CO−$D_2$ coadsorption. The curves resulting from the temperature-programmed heating of pristine samples of the catalyst and its CB support under vacuum (without any chemisorbed probe) are also included as references. Several striking features can be appreciated in the resulting profiles. The broad desorption bands ob-

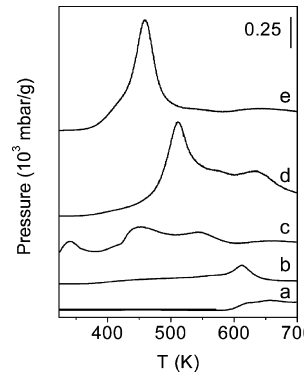


**FIGURE 9. Chamber pressure due to desorbed products during TPD tests in (a) a pristine sample of Vulcan XC72, (b) a pristine sample of the Pt/Vulcan XC72 catalyst, (c) a $D_2$-equilibrated sample, (d) a CO-equilibrated sample, and (e) $D_2$ adsorbed over a CO-equilibrated sample. Adsorption of probes has always been performed on samples previously evacuated at 448 K.**

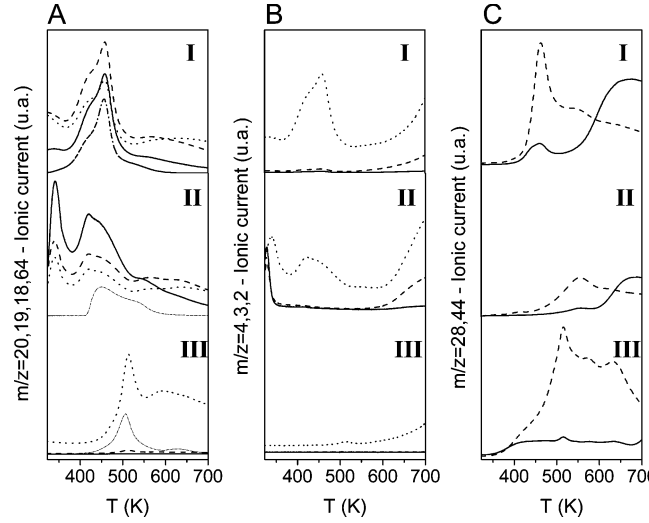


**FIGURE 10. Ion currents obtained for different masses during the TPD tests in samples of the Pt/Vulcan XC72 catalyst equilibrated with (I) CO and $D_2$, (II) $D_2$, and (III) CO. Curves in A: ion currents for *m/z* 20 [$D_2O$ (— —)], 19 [HDO (- - -)], 18 [$H_2$ (· · ·)], and 64 [$SO_2$ (· · ·)]. Curves in B: ion currents for *m/z* 4 [$D_2$ (— —)], 3 [HD (- - -)], and 2 [$H_2$ (· · ·)]. Curves in C: ion currents for *m/z* 28 [CO (— —)] and 44 [$CO_2$ (- - -)].**

tained for the $D_2$-equilibrated sample evidence that only a part of the adsorbed $H_2$ is on the Pt surface. The Pt-chemisorbed $H_2$ originates a low-temperature desorption peak (below 373 K). Large differences can also be found between the profile obtained from the sample in which CO and $D_2$ are coadsorbed and the profiles for the sample equilibrated with CO or $D_2$ separately. The main desorption peak in the coadsorption curve appears at a much lower temperature and the peak corresponding to the Pt-chemisorbed $H_2/D_2$ disappears.

The mass spectrometric analysis of the desorbed species during the TPD tests renders a clearer picture of the surface phenomena taking place in the catalyst after adsorption of these probes. Figure 10 compiles the ionic current curves obtained in each case for the formation of labeled $H_2O$ and $SO_2$ (Figure 10A), labeled molecular $H_2$ (Figure 10B), and carbon oxides (CO and $CO_2$; Figure 10C). It can be observed that $H_2O$ desorption above 373 K is in all cases associated

with the release of $SO_2$, which proceeds from decomposition of sulfonic groups. It must be noted that, when no adsorbed probe is present on the catalyst, the $SO_2$ release curve presents three contributions above 448 K with a predominant maximum at ca. 600 K (Figure 4). This profile is drastically modified after adsorption of CO, $D_2$, or both. Adsorbed CO causes sulfonic groups to reduce their main decomposition maximum to 507 K (Figure 10A-III). This process is also associated with the formation of large amounts of $CO_2$ (Figure 10C-III) instead of the reversible release of the adsorbed probe (CO). It evidences the interaction of the adsorbed CO molecules with the support hydrophilic sulfonic groups, which contribute to their oxidation before being desorbed. Just a small amount of $H_2$ resulting from the decomposition of some $CH_x$ species in the support is detected at temperatures above 500 K (Figure 10B-III). A similar $H_2$ evolution profile can be observed in the TPD test for the pristine catalyst (Figure 4).

The analyses of the labeled species desorbed from the $D_2$- and $D_2$−CO-equilibrated samples reveal several important details on the interaction of the adsorbates with the catalyst surface.

In the $D_2$-equilibrated sample, the release of molecular $H_2$ isotopes confirms the spillover phenomenon (Figure 10B-II): three main desorption bands are observed, with the main contribution being that of $H_2$ (*m*/*z* 2). $H_2$ desorption taking place at low temperature (below 373 K) is usually associated with dissociated $H_2$ species chemisorbed on the Pt surface: the most weakly adsorbed species are released as $D_2$ (*m*/*z* 4) and HD (*m*/*z* 3), whereas $H_2$ is also formed from Pt-adsorbed species resulting from the exchange with $H_2$ from the support surface groups. The desorption peak appearing within the 400−500 K range arises only from $H_2$, showing no contribution of the heavier isotopes. It probably results from the recombination of $H_2$ species in direct interaction with sulfonic groups, which are released simultaneously with $H_2O$ and $SO_2$. The third peak appearing above 600 K is typical from $H_2$ spilled-over species in interaction with the support surface in supported metals. Although the ion current for mass 2 ($H_2$) is the main contribution to that peak, the ion current increase for mass 3 in that temperature range reveals the presence of labeled species remaining on the support, which are recombined at high temperature to be released as HD.

The $H_2O$ desorption profiles for the $D_2$-equilibrated sample indicate that the spillover phenomenon and the presence of $H_2O$ as the proton acceptor are intimately related because most of the adsorbed D atoms are finally released in two main peaks in the form of isotopically labeled $H_2O$ (Figure 10A-II). These peaks concur with the molecular $H_2$ desorption processes at low and medium temperatures, with $D_2$ and HD being their main contributions. It must be noted that there is some CO and $CO_2$ desorption (Figure 10C-II) resulting from the decomposition of surface groups, as was previously seen in Figure 4 for the TPD test in the pristine catalyst. Although $CO_2$ release takes place simultaneously with that of $SO_2$ in the absence of adsorbates, these processes are decoupled after adsorbing $D_2$ on the sample.

The TPD test on the catalyst where $D_2$ has been adsorbed over the CO-equilibrated sample provides new evidence on the $H_2$ spillover process. The profiles for molecular $H_2$ isotopes indicate that the Pt surface is able to catalyze the $D_2$ dissociation and diffusion toward the support, even when the Pt surface sites are blocked for $H_2$ adsorption on it (Figure 10B-I). Thus, molecular $H_2$ evolution is just observed above 373 K. Only $H_2$ is observed in the intermediate range 373−500 K, whereas $H_2$ and HD appear above 600 K. The absence of any molecular $H_2$ formation below 373 K indicates that the Pt surface is occupied by adsorbed CO at those temperatures. Regarding the competitive adsorption of $H_2$ and CO, Meland and Kjelstrup (91) have found similar results in a study about the influence of CO poisoning of the anode in a PEMFC using electrochemical impedance spectroscopy. They observed that, although CO hinders $H_2$ access to the surface by occupying it and by making it more polarizable, the proton hydration step to diffuse toward the membrane is relatively unaffected by its presence.

In the TPD obtained after coadsorption, HDO, $D_2O$, and $H_2O$ are formed simultaneously with $H_2$ at intermediate temperatures. This indicates that most of the adsorbed $D_2$ is finally released as $H_2O$ (Figure 10A-I). Adsorbed CO is released mainly as $CO_2$ in a peak with a maximum at 460 K, which concurs with the most intense contribution for $H_2O$ and $SO_2$ formation. At temperatures above 530 K, $H_2O$ desorption is practically depleted and $CO_2$ formation decreases in favor of CO (39).

An issue requiring special attention is the lability of the Vulcan XC72 surface S species, which experiences a significant change depending on the adsorbates on the catalyst. It is worth noting that at least three types of S species with different stabilities are observed to contribute to the ion current curves for mass *m*/*z* 64 in the several TPD tests performed for the pristine sample and those equilibrated with CO, $D_2$, or both. A comparison of the $SO_2$ release curve in the $D_2$−CO-equilibrated sample (Figure 10A-I) with those corresponding to the tests after $D_2$ or CO adsorption (Figure 10A-II,III) evidence modification of the stability of the surface S species formed. The main difference lies in the decrease of the $SO_2$ release temperature. Although its formation always remains associated with $H_2O$ removal, the $SO_2$ appearance begins at temperatures below 373 K when $D_2$ and CO are coadsorbed.

It is clear from the results that the adsorbed probes have a major interaction with the S surface groups. They also probably interact with the F-containing species attached to Vulcan XC72. By analysis of the ion current for mass *m*/*z* 31, attributable to the $CF^+$ fragment (see Figure 3), the fluorided species release could also be followed. In the case of $D_2$−CO coadsorption, the release temperature of those fluorinated groups is observed to decrease by 245 K, yielding a peak for the $CF^+$ fragment at 440 K (not shown).

The low decomposition temperature for S surface groups in the presence of $H_2$ and CO has several implications in the

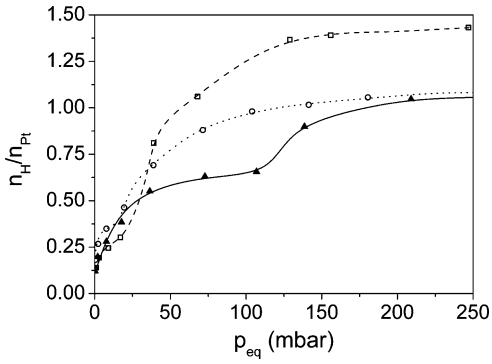


FIGURE 11. $H_2$ adsorption isotherms obtained for different GDEs (0.5 $mg_{Pt} \cdot cm^{-2}$) containing Pt/Vulcan XC72: (···○···) a homemade GDE prepared by manual impregnation of an isopropyl alcohol based ink on a woven gas diffusion medium; (- - -□- - -) a homemade GDE prepared by manual impregnation of a glycerol-containing ink on a woven gas diffusion medium; (—▲—) a commercial LT-140E-W ELAT GDE.

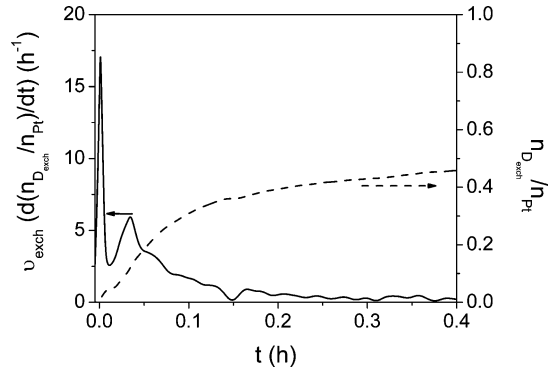


FIGURE 12. $D_2/H_2$ exchange frequency ($\nu_{exch}$) (solid line) and amount of moles of exchanged D atoms per mol of Pt (dotted line) in the commercial GDE as a function of the contact time between the gas and sample at 298 K. The catalyst had been previously treated under dynamic vacuum at 448 K for 1 h.

stability of catalytic layers during fuel cell operation. CO contamination of the electrocatalyst is a potential cause of degradation that can be easily avoided in most cases. The impact of the presence of CO in the PEMFC anode feeding is fairly well-known and studied and is considered to be most likely reversible (92). However, it can be inferred from the TPD results that the presence of CO in a $H_2$ stream fed to a fuel cell anode may accelerate the degradation of catalysts containing some surface groups on its surface such as hydrophilic S species. As a matter of fact, surface groups in Vulcan XC72 resemble those present in the perfluorosulfonic acid ionomer commonly used in catalytic layers. The effect of CO contamination on the ionomer sulfonic groups close to Pt particles could possibly be very similar to those observed in the Pt/Vulcan XC72 catalyst surface groups, but verification of this assumption needs further research.

**$H_2$ Adsorption and Proton-Exchange Rate on GDEs with Pt/Vulcan XC72.** Additional tests were carried out with GDEs containing Pt/Vulcan XC72 in the catalytic layer for comparison purposes. The GDEs were pretreated under vacuum at 448 K before adsorption or exchange at 298 K, in the same way as the catalyst. $H_2$ adsorption isotherms on the GDEs showed at least two distinguishable plateaus at increasing equilibrium pressures, as can be noted in Figure 11. The isotherm profile variation probably depends on the coverage of the Pt surface by the perfluorosulfonic ion-exchange resin and the interaction between them. The two plateaus could be ascribed to the different $H_2$ adsorption/diffusion rates over the free Pt particles on the support or over Pt particles on Vulcan XC72, which are covered by the resin or in close interaction with it. Considering that the two homemade GDEs have been prepared with the previously analyzed Pt/Vulcan XC72 catalyst, it is clear that the presence of the ion-exchange resin introduces additional difficulties to the determination of the exposed Pt surface area by means of $H_2$ chemisorption. In a previous study, the influence of using catalytic inks with different solvents on the catalytic layer microstructure and performance of the prepared electrodes was shown (93). During the catalytic layer deposition process, the Nafion dispersion recasts in different configurations, which depend on the solvent composition and its evaporation rate. Thus, the Pt/Nafion interface, the size of the Nafion aggregates, and the catalyst coverage will also determine the effective perimeter in the Pt particles for $H_2$ surface diffusion.

The $H_2$ adsorption results in relation to the Pt surface area suggest that, in general, widely used data on the electrochemically active surface area and Pt utilization in the catalyst layers should be corrected for the effects of the support, which may store a significant amount of adsorbed $H_2$, and the ionomer. Paulus et al. reported a fundamental investigation regarding the catalyst utilization at the electrode/membrane interface (94). They compared GDEs (Pt black on C paper and Pt/C on a woven gas diffusion medium) with model electrodes designed by covering glassy C with continuous or discontinuous Pt films. In agreement with our results, their study reveals that the $H_2$ adsorption/desorption characteristics and the catalyst surface utilization depend on the nature of the catalyst in the electroactive layer and the pretreatment applied to the GDEs. In all those cases, the degree of Pt utilization is observed to decrease when increasing the sweep rate during cyclic voltammetry, phenomena that are explained in terms of diffusion of adsorbed species on the Pt surface and surface conductivity in the electrolyte films. Accounting for this effect, Neyerling et al. developed an analytical model to describe the effective proton resistance in the porous cathode electrode of a PEMFC based on a quick and accurate evaluation of cathode proton resistance by using in situ perturbation measurements (95). The model they proposed serves as a guideline of experimental design parameters such that catalyst utilization is kept above 90%, which is a prerequisite for measuring the $O_2$ reduction reaction kinetics.

The $D_2$ exchange rate has also been analyzed in the commercial GDE after heat treatment under vacuum at 448 K. Figure 12 shows the $D_2$ exchange rate and the moles of exchanged D atoms in the GDE as a function of time. In this case, the proportion the surface Pt in the catalyst has not been determined. Therefore, the exchange rate refers to the total amount of Pt in the electrode.

Three processes occurring at different rates can be distinguished during the $D_2$ exchange with the GDE, while only the two slower ones were observed during the exchange with the bare catalyst. The occurrence of a very fast exchange at short times can be ascribed to the presence of the proton-exchange resin in the vicinity of some Pt crystallites. The second and third exchange processes can be assigned to those previously seen for the catalyst itself with the support surface groups, although their rate referring to the Pt (or surface Pt) in the electrode is probably influenced by the presence of the ion-exchange resin.

The mass spectrometric analysis of the isotopic composition of the gas phase during the exchange process allows calculation of the surface diffusion coefficient of $D_2$ in the samples by representing the evolution of the exchanged atoms ($N_e^t$) as a function of $\sqrt{t}$. When the surface migration is the rate-determining step of the exchange, the measured rate depends on both the coefficient of surface diffusion ($D_s$) and the specific perimeter ($I_0$) of the metal particles, which are the sources of dissociated $D_2$ species. Considering the Pt particles to have a semispherical geometry and upon application of the model proposed by Kramer and Andre (96), which has been also used by Cavanagh and Yates (97) and by Duprez and Miloudi (98), the number of atoms diffused ($N_e^t$) at the beginning of exchange reaction (when the concentration of labeled species is constant) can be estimated according to eq 1:

$$N_e^t = \frac{2}{\pi} C_D I_0 \sqrt{D_s t} \quad \text{with } I_0 = N_p(2\pi r) \tag{1}$$

where $C_D$ is the atomic concentration of the labeled species ($at \cdot m^{-2}$), $r$ is the average radius of the metal particles (m), and $I_0$ is the length of the metal−support interface, i.e., the total perimeter of the metal particle per $m^2$ of catalyst ($m \cdot m^{-2}$). Assuming that the adsorption/desorption of $D_2$ is very fast and that the direct exchange of $D_2$ with the support is negligible at the experimental temperature, the coefficient of surface diffusion could be calculated by the following eq 2:

$$D_s = \left(\frac{\pi}{4}\right)\left(\frac{S_1}{C_D I_0}\right) \quad \text{with } S_1 = \frac{dN_e^t}{d\sqrt{t}} \tag{2}$$

where $S_1$ is the initial slope of the curve representing the variation of $N_e^t$ as a function of $\sqrt{t}$. The fitting of the experimental data to the model yields values of $7.77 \times 10^7$ $m \cdot m^{-2}$ for the metal−support interface ($I_0$) in the catalyst and a surface diffusion coefficient ($D_s$) of $1.63 \times 10^{-19}$ $m^2 \cdot s^{-1}$. In the GDE, the surface diffusion coefficient increases by 3 orders of magnitude up to $1.83 \times 10^{-16}$ $m^2 \cdot s^{-1}$ with a particle perimeter length ($I_0$) of $12.37 \times 10^7$ $m \cdot m^{-2}$. It must be taken into consideration that the isotopic exchange has been performed in the samples after their treatment at a temperature high enough to remove practically all of the adsorbed $H_2O$ without decomposition of the support surface groups. In that way, those groups containing in their structure exchangeable $H_2$ can be evaluated without contribution of the $D_2$ exchange with $H_2O$ molecules. A rough estimation of the amount of exchanged $H_2$ associated with surface groups in the studied catalyst within a period of 0.4 h yields approximately a value of $5 \times 10^{-6}$ $mol \cdot m^{-2}$. This amount is reduced to $3.5 \times 10^{-6}$ $mol \cdot m^{-2}$ in the case of the commercial GDE. The addition of the proton-exchange resin to the catalytic layer increases the proton-exchange rate in the vicinity of Pt particles but blocks some groups of the support that could participate in the proton surface diffusion. A challenging breakthrough for improving the proton-transfer pathways between the electrodes and the ion-exchange membrane consists of designing tailor-made supports that are chemically modified with adequate proton acceptor groups to provide high $H_2$ surface diffusion coefficients.

## CONCLUSIONS

The adsorption and exchange properties of a Pt/Vulcan XC72 catalyst have been studied by applying adsorption, desorption, and exchange techniques with $H_2$, $D_2$, and CO as probes. The obtained results indicate that the presence of hydrophilic sulfonic groups associated with the CB induces a spillover process that favors $H_2$ adsorption in large amounts on the catalyst. The chemisorbed $D_2$ is susceptible to being exchanged with labile $H_2$ species associated with some support surface groups. This $D_2$ exchange process seems to take place in two steps under isothermal conditions. The first one can be attributed to the initial chemisorbed monolayer, which is readily exchanged with CB surface species in a fast process. In a second step, the exchange reaches a steady state whose rate probably depends on a slower $H_2$ surface diffusion process on the CB surface.

The interaction of adsorbates such as $D_2$ or CO with the S-containing surface species has been evidenced by means of TPD tests of adsorbed probes. Coadsorption of both CO and $D_2$ has revealed that preadsorbed CO blocks Pt surface sites for $D_2$ chemisorption on them, but the pathways for surface diffusion of $D_2$ toward the support remain operative.

The S-containing groups in the support are thermally stable under an inert atmosphere at temperatures up to 448 K in the absence of adsorbates such as $H_2$ or CO. Above that temperature, they decompose by releasing $H_2O$ and $SO_2$ as the main degradation products. In the presence of adsorbates, the thermal stability of those species is reduced. In particular, coadsorption of both CO and $D_2$ reduces the decomposition temperature for sulfonic groups below 373 K. This may lead to an irreversible degradation of the catalyst properties with regards to proton mobility.

By a comparison of the $H_2$ adsorption processes taking place in the Pt/Vulcan XC72 catalyst with those occupying a GDE containing that type of catalyst, it has been observed that the presence of an ion-exchange resin distributed within the catalytic layer modifies the $H_2$ adsorption behavior of the sample. The observed changes seem to depend on the amount and distribution of the resin, inducing a faster exchange process with $D_2$ and partially modifying the slower exchange with the surface groups of the catalyst support.

The participation of the surface chemistry of PEMFC catalyst supports can be analyzed in light of these results. The surface modification of C materials as catalytic supports may provide an effective pathway to developing new catalysts for an enhanced performance of GDEs, providing faster proton mobility and better stability of surface groups throughout the catalytic layer while reducing the amount of ion-exchange resin in it.

**Acknowledgment.** The author thanks the Spanish Ministry for Education and Science and the Comunidad de Madrid for financial support under Projects MEDEA (ENE2005-08799-C02-01/ALT) and ENERCAM-CM (S-0505/ENE-304), respectively, and the Fuel Cells group from ICP-CSIC and the Unit for Fuel Cells and Systems Integration from CIEMAT for their support.

**Supporting Information Available:** Characterization data including a comparison of the average particle sizes from $H_2$ chemisorption, TEM statistical analysis, and broadening of the Pt XRD lines, XRD profiles and TEM micrographs from the catalyst, and characteristic parameters estimated for the catalyst and the GDE from the adsorption/exchange experiments based on the model of Kramer and Andre (96). This material is available free of charge via the Internet at http://pubs.acs.org.

## REFERENCES AND NOTES

(1) Kinoshita, K. *Carbon*; Wiley: New York, 1998.
(2) Kim, H.; Park, J.-N.; Lee, W.-H. *Catal. Today* **2003**, *87* (1−4), 153.
(3) Smirnova, A.; Dong, X.; Hara, H.; Vasiliev, A.; Sammes, N. *Int. J. Hydrogen Energy* **2005**, *30*, 149.
(4) Babic, B. M.; Vracar, L. M.; Radmilovic, V.; Krstajic, N. V. *Electrochim. Acta* **2006**, *51*, 3820.
(5) Kim, M.; Park, J.-N.; Kim, H.; Song, S.; Lee, W.-H. *J. Power Sources* **2006**, *163*, 93.
(6) He, H.; Klinowski, J.; Forster, M.; Lerf, A. *Chem. Phys. Lett.* **1998**, *287*, 53.
(7) Carmo, M.; Paganin, V. A.; Rosolen, J. M.; Gonzalez, E. R. *J. Power Sources* **2005**, *142*, 169.
(8) Lee, K.; Zhang, J.; Wang, H.; Wilkinson, D. P. *J. Appl. Electrochem.* **2006**, *36*, 507.
(9) Guha, A.; Zawodzinski, T. A., Jr.; Schiraldi, D. A. *J. Power Sources* **2007**, *172*, 530.
(10) Yoshitake, T.; Shimakawa, Y.; Kuroshima, S.; Kimura, H.; Ichihashi, T.; Kubo, Y.; Kasuya, D.; Takahashi, K.; Kokai, F.; Yudasaka, M.; Iijima, S. *Phys. B* **2002**, *323*, 124.
(11) Hyeon, T.; Han, S.; Sung, Y.-E.; Park, K.-W.; Kim, Y.-W. *Angew. Chem., Int. Ed.* **2003**, *42*, 4352.
(12) Yu, J.-S.; Kang, S.; Yoon, S. B.; Chai, G. *J. Am. Chem. Soc.* **2002**, *124*, 9382.
(13) Wang, X.; Li, W.; Chen, Z.; Waje, M.; Yan, Y. *J. Power Sources* **2006**, *158*, 154.
(14) Marie, J.; Berthon-Fabry, S.; Achard, P.; Chatenet, M.; Pradourat, A.; Chainet, E. *J. Non-Cryst. Solids* **2004**, *350*, 88.
(15) McCreery, R. L. *Chem. Rev.* **2008**, *108* (7), 2646.
(16) Santiago, E. I.; Varanda, L. C.; Villullas, H. M. *J. Phys. Chem. C* **2007**, *111*, 3146.
(17) Fang, B.; Kim, J. H.; Lee, C.; Yu, J. S. *J. Phys. Chem. C* **2008**, *112*, 639.
(18) Hui, C. L.; Li, X. G.; Hsing, I. M. *Electrochim. Acta* **2005**, *51*, 711.
(19) Pozio, A.; de Francesco, M.; Cemmi, A.; Cardellini, F.; Giorgi, L. *J. Power Sources* **2002**, *105*, 13.
(20) Stevens, D. A.; Dahn, J. R. *J. Electrochem. Soc.* **2003**, *150* (6), A770.
(21) Gasteiger, H. A.; Kocha, S. S.; Sompalli, B.; Wagner, F. T. *Appl. Catal. B: Environ.* **2005**, *56*, 9.
(22) Tamizhmani, G.; Dodelet, J. P.; Guay, D. *J. Electrochem. Soc.* **1996**, *143* (1), 18.
(23) Fournier, J.; Faubert, G.; Tilquin, J. Y.; Côté, R.; Guay, D.; Dodelet, J. P. *J. Electrochem. Soc.* **1997**, *144* (1), 145.
(24) Schmidt, T. J.; Gasteiger, H. A.; Stäb, G. D.; Urban, P. M.; Kolb, D. M.; Behm, R. J. *J. Electrochem. Soc.* **1998**, *145* (7), 2354.
(25) Perez, J.; Tanaka, A. A.; Gonzalez, E. R.; Ticianelli, E. A. *J. Electrochem. Soc.* **1994**, *141*, 431.
(26) Paulus, U. A.; Wokaun, A.; Scherer, G. G.; Schmidt, T. J.; Stamenkovic, V.; Markovic, N. M.; Ross, P. N. *Electrochim. Acta* **2002**, *47*, 3787.
(27) Perez, J.; Gonzalez, E. R.; Ticianelli, E. A. *Electrochim. Acta* **1998**, *44* (8−9), 1329.
(28) Gloaguen, F.; Andolfatto, F.; Durand, R.; Ozil, P. *J. Appl. Electrochem.* **1994**, *24* (9), 863.
(29) Ciureanu, M.; Wang, H. *J. Electrochem. Soc.* **1999**, *146* (11), 4031.
(30) Mukerjee, S.; Srinivasan, S. *J. Electroanal. Chem.* **1993**, *357* (1−2), 201.
(31) Lee, S. J.; Mukerjee, S.; McBreen, J.; Rho, Y. W.; Kho, Y. T.; Lee, T. H. *Electrochim. Acta* **1998**, *43* (24), 3693.
(32) Xie, Z.; Navessin, T.; Shi, K.; Chow, R.; Wang, Q.; Song, D.; Andreaus, B.; Eikerling, M.; Liu, Z.; Holdcroft, S. *J. Electrochem. Soc.* **2005**, *152* (6), A1171.
(33) Bansal, R. C.; Donnet, J.-B. In *Carbon Black: Science and Technology*; Donnet, J.-B., Bansal, R. C., Wang, M. J., Eds.; Marcel Dekker Inc.: New York, 1993; Chapter 4.
(34) Poleunis, C.; Vanden Eynde, X.; Grivei, E.; Smet, H.; Probst, N.; Bertrand, P. *Surf. Interface Anal.* **2000**, *30*, 420.
(35) Cameron, D. S.; Cooper, S. J.; Dodgson, I. L.; Harrison, B.; Jenkins, J. W. *Catal. Today* **1990**, *7*, 113.
(36) Kangasniemi, K. H.; Condit, D. A.; Jarvi, T. D. *J. Electrochem. Soc.* **2004**, *151* (4), E125.
(37) Zhang, Y. J.; Maroto-Valiente, A.; Rodriguez-Ramos, I.; Xin, Q.; Guerrero-Ruiz, A. *Catal. Today* **2004**, *93−95*, 619.
(38) Baturina, O. A.; Aubuchon, S. R.; Wynne, K. J. *Chem. Mater.* **2006**, *18*, 1498.
(39) Ferreira-Aparicio, P. *Chem. Mater.* **2007**, *19*, 6030.
(40) Antonucci, P. L.; Alderucci, V.; Giordano, N.; Cocke, D. L.; Kim, H. *J. Appl. Electrochem.* **1994**, *24* (1), 58.
(41) Yu, X.; Ye, S. *J. Power Sources* **2007**, *172*, 133, and references cited therein.
(42) Yu, X.; Ye, S. *J. Power Sources* **2007**, *172*, 145.
(43) Dicks, A. L. *J. Power Sources* **2006**, *156*, 128.
(44) Park, C. H.; Scibioh, M. A.; Kim, H.-J.; Oh, I.-H.; Hong, S.-A.; Ha, H. Y. *J. Power Sources* **2006**, *162*, 1023.
(45) Bezerra, C. W. B.; Zhang, L.; Liu, H.; Lee, K.; Marques, A. L. B.; Marques, E. P.; Wang, H.; Zhang, J. *J. Power Sources* **2007**, *173*, 891.
(46) Stevens, D. A.; Dahn, J. R. *Carbon* **2005**, *43*, 179.
(47) Ferreira-Aparicio, P. *Electrochem. Solid-State Lett.* **2009**, *12* (3), B38.
(48) Borup, R.; Meyers, J.; Pivovar, B.; Kim, Y. S.; Mukundan, R.; Garland, N.; Myers, D.; Wilson, M.; Garzon, F.; Wood, D.; Zelenay, P.; More, K.; Stroh, K.; Zawodzinski, T.; Boncella, J.; McGrath, J. E.; Inaba, M.; Miyatake, K.; Hori, M.; Ota, K.; Ogumi, Z.; Miyata, S.; Nishikata, A.; Siroma, Z.; Uchimoto, Y.; Yasuda, K.; Kimijima, K.; Iwashita, N. *Chem. Rev.* **2007**, *107*, 3904.
(49) Shao, Y.; Yin, G.; Gao, Y. *J. Power Sources* **2007**, *171*, 558.
(50) Shao, Y.; Yin, G.; Wang, Z.; Gao, Y. *J. Power Sources* **2007**, *167*, 235.
(51) Shao, Y.; Liu, J.; Wang, Y.; Lin, Y. *J. Mater. Chem.* **2009**, *19*, 46.
(52) Zhang, S.; Yuan, X.; Wang, H.; Mérida, W.; Zhu, H.; Shen, J.; Wu, S.; Zhang, J. *Int. J. Hydrogen Energy* **2009**, *34*, 388.
(53) Du, C. Y.; Zhao, T. S.; Liang, Z. X. *J. Power Sources* **2008**, *176*, 9.
(54) Xu, Z.; Qi, Z.; Kaufman, A. *Electrochem. Solid-State Lett.* **2003**, *6* (9), A171.
(55) Xu, Z.; Qi, Z.; Kaufman, A. *Electrochem. Solid-State Lett.* **2005**, *8* (6), A313.
(56) Joo, S. H.; Pak, C.; Kim, E. A.; Lee, Y. H.; Chang, H.; Seung, D.; Choi, Y. S.; Park, J.-B.; Kim, T. K. *J. Power Sources* **2008**, *180*, 63.
(57) Scibioh, M. A.; Oh, I.-H.; Lim, T.-H.; Hong, S.-A.; Ha, H. Y. *Appl. Catal. B: Environ.* **2007**, *77*, 373.
(58) Pozio, A.; Silva, R. F.; De Francesco, M.; Giorgi, L. *Electrochim. Acta* **2003**, *48*, 1543.
(59) Cai, M.; Ruthkosky, M. S.; Merzougui, B.; Swathirajan, S.; Balogh, M. P.; Oh, S. H. *J. Power Sources* **2006**, *160*, 977.
(60) Coloma, F.; Escribano, A. S.; Fierro, J. L. G.; Rodríguez-Reinoso, F. *Langmuir* **1994**, *10*, 750.
(61) Jiang, M.; Ning, Z. *J. Non-Cryst. Solids* **2005**, *351*, 2462.
(62) Yokomichi, H.; Masuda, A. *J. Non-Cryst. Solids* **2000**, *271*, 147.

(63) Xin, Y.; Ning, Z. Y.; Ye, C.; Lu, X. H.; Xiang, S. L.; Du, W.; Huang, S.; Chen, J.; Cheng, S. H. *Surf. Coat. Technol.* **2003**, *173*, 172.
(64) Stelmashuka, V.; Biederman, H.; Slavýnska, D.; Zemek, J.; Trchova, M. *Vacuum* **2005**, *77*, 131.
(65) Lappan, U.; Geissler, U.; Uhlmann, S. *Nucl. Instrum. Methods Phys. Res., Sect. B* **2005**, *236*, 413.
(66) Asano, S.; Mutou, F.; Ichizuri, S.; Li, J.; Miura, T.; Oshima, A.; Katsumura, Y.; Washio, M. *Nucl. Instrum. Methods Phys. Res., Sect. B* **2005**, *236*, 437.
(67) Njatawidjaja, E.; Kodama, M.; Matsuzaki, K.; Yasuda, K.; Matsuda, T.; Kogoma, M. *Surf. Coat. Technol.* **2006**, *201*, 699.
(68) Liang, Z.; Chen, W.; Liu, J.; Wang, S.; Zhou, Z.; Li, W.; Sun, G.; Xin, Q. *J. Membr. Sci.* **2004**, *233*, 39.
(69) Chen, C.; Levitin, G.; Hess, D. W.; Fuller, T. F. *J. Power Sources* **2007**, *169*, 288.
(70) Di Noto, V.; Gliubizzi, R.; Negro, E.; Vittadello, M.; Pace, G. *Electrochim. Acta* **2007**, *53*, 1618.
(71) Laporta, M.; Pegoraro, M.; Zanderighi, L. *Phys. Chem. Chem. Phys.* **1999**, *1*, 4619.
(72) Ostrowska, J.; Narebska, A. *Colloid Polym. Sci.* **1983**, *261* (2), 93.
(73) Ostrowska, J.; Narebska, A. *Colloid Polym. Sci.* **1984**, *262* (4), 305.
(74) Socrates, C. *Infrared Characteristic Frequencies*; Wiley Interscience: New York, 1980.
(75) Nakahara, M.; Sanada, Y. *J. Mater. Sci.* **1995**, *30*, 4363.
(76) Lakshmi, N.; Rajalakshmi, N.; Dhathathreyan, K. S. *J. Phys. D: Appl. Phys.* **2006**, *39*, 2785.
(77) Artyushkova, K.; Fulghum, J. E. *Surf. Interface Anal.* **2001**, *31*, 352.
(78) Wilson, D. J.; Williams, R. L.; Pond, R. C. *Surf. Interface Anal.* **2001**, *31*, 397.
(79) Vesel, A.; Mozetic, M.; Zalar, A. *Surf. Interface Anal.* **2007**, *40* (3−4), 661.
(80) Ramdutt, D.; Charles, C.; Hudspeth, J.; Ladewig, B.; Gengenbach, T.; Boswella, R.; Dicks, A.; Brault, P. *J. Power Sources* **2007**, *165*, 41.
(81) Lin, H. Y.; Chen, W.-C.; Yuan, C.-S.; Hung, C.-H. *J. Air Waste Manage. Assoc.* **2008**, Jan, doi: 10.3155-1047-3289.58.1.78.
(82) Caro, J. C.; Lappan, U.; Lunkwitz, K. *Surf. Coat. Technol.* **1999**, *116−119*, 792.
(83) Schulze, M.; Lorenz, M.; Wagner, N.; Gülzow, E. *Fresenius' J. Anal. Chem.* **1999**, *365*, 106.
(84) Anderson, J. R. *Structure of metallic catalysts*; Academic Press: New York, 1975; pp 295−297.
(85) Podkolzin, S. G.; Shen, J.; de Pablo, J. J.; Dumesic, J. A. *J. Phys. Chem.* **2000**, *B 104*, 4169.
(86) Liu, W.-J.; Wu, B.-L.; Cha, C.-S. *J. Electroanal. Chem.* **1999**, *476* (2), 101.
(87) Ramirez-Cuesta, A. J.; Mitchell, P. C. H.; Parker, S. F.; Tomkinson, J.; Thompsett, D. *Stud. Surf. Sci. Catal.* **2001**, *138*, 55.
(88) Mitchell, P. C. H.; Ramirez-Cuesta, A. J.; Parker, S. F.; Tomkinson, J.; Thompsett, D. *J. Phys. Chem. B* **2003**, *107* (28), 6838.
(89) Hampden-Smith, M.; Carusso, J.; Atanassova, P.; Kyrlidis, A. (Cabot Corp.). Surface modified carbon products and their application. Patent WO2005090486, 2005.
(90) Kosbach L.; Yu, Y. (Cabot Corp.). Modified carbon products useful in gas diffusion electrodes. Patent WO0128015 (A1), 2001.
(91) Meland, A.-K.; Kjelstrup, S. *J. Electroanal. Chem.* **2007**, *610*, 171.
(92) Fowler, M.; Amphlett, J. C.; Mann, R. F.; Peppley, B. A.; Roberge, P. R. *J. New. Mater. Electrochem. Syst.* **2002**, *5*, 255.
(93) Fernández, R.; Ferreira-Aparicio, P.; Daza, L. *J. Power Sources* **2005**, *151*, 18.
(94) Paulus, U. A.; Veziridis, Z.; Schnyder, B.; Kuhnke, M.; Scherer, G. G.; Wokaun, A. *J. Electroanal. Chem.* **2003**, *541*, 77.
(95) Neyerlin, K. C.; Gu, W.; Jorne, J.; Clark, A., Jr.; Gasteiger, H. A. *J. Electrochem. Soc.* **2007**, *154* (2), B279.
(96) Kramer, R.; Andre, M. *J. Catal.* **1979**, *58*, 287.
(97) Cavanagh, R. R.; Yates, J. T., Jr. *J. Catal.* **1981**, *68*, 22.
(98) Duprez, D.; Miloudi, A. *Stud. Surf. Sci. Catal.* **1983**, *17*, 298.

AM9003446